Available online at www.sciencedirect.com
SCIENCE DIRECT®
C. R. Mecanique 331 (2003) 843–848
COMPTES RENDUS MECANIQUE

Using data assimilation in numerical simulations of experimental geophysical flows

Martin Galmiche, Joël Sommeria, Emmanuelle Thivolle-Cazat, Jacques Verron

Laboratoire des écoulements géophysiques et industriels, BP 53, 38041 Grenoble cedex 9, France

Received 25 February 2003; accepted after revision 14 October 2003

Presented by René Moreau

Abstract

Data assimilation is used to couple numerical simulations and laboratory experiments of unsteady fluid flows in a stratified, rotating fluid. The experiments are performed on the large Coriolis turntable (Grenoble) and the simulations are performed with a multi-layer shallow water model. Sequential assimilation of high-resolution CIV (Correlation Image Velocimetry) measurements drives the numerical model close to the experimental flow and provides an estimation of all the flow variables at each time and each point. It is then possible (i) to analyse the flow dynamics in details, (ii) to determine the model errors starting from a realistic initial condition and (iii) to test the assimilation scheme when a reduced set of data is assimilated. To illustrate this, some results on the baroclinic instability of a two-layer vortex are presented. ***To cite this article: M. Galmiche et al., C. R. Mecanique 331 (2003).***

Résumé

Assimilation de données pour la simulation numérique d'écoulements géophysiques expérimentaux. L'assimilation de données est utilisée pour coupler simulation numérique et mesure expérimentale d'écoulements stratifiés transitoires en milieu tournant. Les expériences sont réalisées sur la grande Plaque Coriolis (Grenoble) et les simulations sont effectuées à l'aide d'un modèle shallow water multi-couches. L'assimilation séquentielle des mesures CIV (Vélocimétrie par Corrélation d'Images de particules) haute résolution permet de contraindre le modèle numérique par l'écoulement expérimental et fournit une estimation de toutes les variables, en chaque point et à chaque instant. Il est alors possible (i) d'analyser en détail la dynamique de l'écoulement, (ii) de déterminer les erreurs modèle à partir d'une condition initiale réaliste et (iii) de tester le schéma d'assimilation lorsqu'un ensemble réduit de données est assimilé. L'exemple de l'instabilité barocline d'un tourbillon bi-couche est présenté. ***Pour citer cet article : M. Galmiche et al., C. R. Mecanique 331 (2003).***

Keywords: Computational fluid mechanics; Data assimilation; Laboratory experiments; Baroclinic instability

Mots-clés : Mécanique des fluides numérique ; Assimilation de données ; Expériences de laboratoire ; Instabilité barocline

E-mail address: martin.galmiche@coriolis-legi.org (M. Galmiche).

1631-0721/$ – see front matter
doi:10.1016/j.crme.2003.10.003

1. Introduction

The heart of ocean and atmosphere forecasting systems consists of three main components: the observation system, the dynamical model and the data assimilation scheme. The ideal method for validating the overall forecasting system would be to compare results with independent in-situ observations, i.e., observations that are not used in the assimilation process. However, such observations are rare because in-situ surveys are difficult to undertake and extremely expensive. Another problem is that, because assimilation is only approximate, forecast errors may be due not only to the model itself, but also to the temporal growth of imperfections in the initial condition. It is therefore difficult to objectively identify the model errors.

We show in this letter an adaptation of a simplified oceanic forecasting model to the analysis of laboratory flows. Our approach relies on numerical simulation of laboratory experiments in a multi-layer, rotating fluid with data assimilation of the velocity measurements. This method not only is an alternative approach of modelling and assimilation problems, but also opens the way to a better physical analysis of laboratory flows.

2. The Coriolis turntable

Thanks to its large size (13 meter diameter), the Coriolis turntable (Grenoble, France) is a unique facility which enables oceanic flows to be reproduced with a good level of similarity (e.g., Serra et al. [1]). It is possible to come close to inertial regimes, i.e., with limited effects of viscosity and centrifugal forces.

From a technical point-of-view, the major difference with the real ocean is that the measured quantity here is the velocity field in several horizontal planes instead of scalar quantities (salinity, sea surface elevation and temperature) measured only at the surface or along vertical sections. The elevation of the interface between the layers is not measured in the experiments. It is treated as an output of the asssimilation process (see Section 3).

The velocity field is measured in horizontal planes using CIV (Correlation Image Velocimetry): particle tracers are illuminated by a horizontal laser sheet and a camera is used to visualize the particle displacements from above, leading, after numerical treatment, to the horizontal velocity field. The rms measurement error in particle displacement is about 0.2 pixels, as determined by Fincham and Delerce [2], and the errors found in neighboring points are not correlated.

In parallel with these measurements, numerical simulations are performed. The system is modelled as a multi-layer fluid with hydrostatic approximation for which the variables are the horizontal velocity components $u(x, y, i)$ and $v(x, y, i)$, and the layer thickness $h(x, y, i)$, where x and y are the horizontal coordinates and i is the layer index. The basic shallow-water equations are solved using MICOM (Miami Isopycnic Coordinate Ocean Model, Bleck and Boudra [3]) in its simplest version.

The measured velocity field is assimilated into the simulations at each measurement point using an adaptive version of the Singular Evolutive Extended Kalman (SEEK) filter, a method adapted for oceanographic purposes on the basis of the Kalman filter. Each data assimilation provides a new dynamical state which optimally blends the model prediction and the measured data, in accounting for their respective error. At the end of each simulation cycle, the forecast state vector $\mathbf{X}^f$ is replaced by the analysed state vector $\mathbf{X}^a = \mathbf{X}^f + \mathbf{K}[\mathbf{Y}^o - \mathbf{H}\mathbf{X}^f]$, where $\mathbf{Y}^o$ is the observed part of the state vector (i.e., the velocity field in the measurement domain), $\mathbf{H}$ is the observation operator and $\mathbf{K}$ is the Kalman gain defined by $\mathbf{K} = \mathbf{P}^f\mathbf{H}^{\mathrm{T}}[\mathbf{H}\mathbf{P}^f\mathbf{H}^{\mathrm{T}} + \mathbf{R}]^{-1}$. Here, $\mathbf{P}^f$ and $\mathbf{R}$ are the forecast error and observation error covariance matrices respectively. The observation errors are here supposed to be uniform, which is a good approximation in the frame of these CIV measurements (Fincham and Delerce [2]). The multivariate correlations between the variables are described as components on Empirical Orthogonal Functions (EOFs) computed from the model statistics, providing an estimation of $\mathbf{P}^f$. The reader is referred to Pham, Verron and Roubaud [4] and Brasseur, Ballabrera-Poy and Verron [5] for mathematical details.

3. Example: Baroclinic instability of a two-layer vortex

A cylinder of radius $R = 0.5$ m is initially introduced in a two-layer fluid across the interface. A displacement η_0 of the interface is produced inside the cylinder, and at $t = 0$ the cylinder is rapidly removed. A radial gravity current is then initiated, which is deviated by the Coriolis force, resulting in the formation of a vortex in the upper layer after damping of inertial oscillations. A vortex of opposite sign is produced in the lower layer, and the resulting vertical shear is a source of baroclinic instability. The main control parameter in this system is $\gamma = R/R_D$, where R_D is the Rossby deformation radius. The results presented here were obtained with $\gamma = 4$. The vortex then undergoes baroclinic instability which gives rise to splitting into two new vortices.

The velocity field is measured in each layer every 11 s, which is half the observed period of inertial oscillations. Since we are interested in the slow balanced dynamics, we eliminate the residual inertial oscillations by averaging two successive fields for data assimilation. The velocity data obtained are assimilated in the numerical model at each grid point in the measurement domain (2.5 m $\times$ 2.5 m). In the numerical simulations, the system is modelled as a two-layer fluid with a standard biharmonic dissipation term and the simulation domain is 5 m wide (i.e., twice as large as the measurement domain) in order to avoid spurious confinement by boundaries. The simulations are performed using 100^2 or 200^2 grid points in each layer.

A good fit is obtained between the model and the experimental data, as shown in Fig. 1. The irregular shape of the vortex, the position of its center and the presence of residual currents in its vicinity are well represented. The elongation of the vortex and the formation of two new, smaller vortices are also well reproduced. Data assimilation provides with an indirect measurement of the interface depth, also shown in Fig. 1.

The initial development of baroclinic instability is well described by the growth of mode two (calulated using a polar Fourier decomposition of the radial velocity field along a circle of radius R). As shown in Fig. 2(a), the growth of this mode is considerably delayed in the model without data assimilation, as the initial perturbation is smaller than in the experiments. When data assimilation is performed, excellent agreement between the model and the observation is obtained.

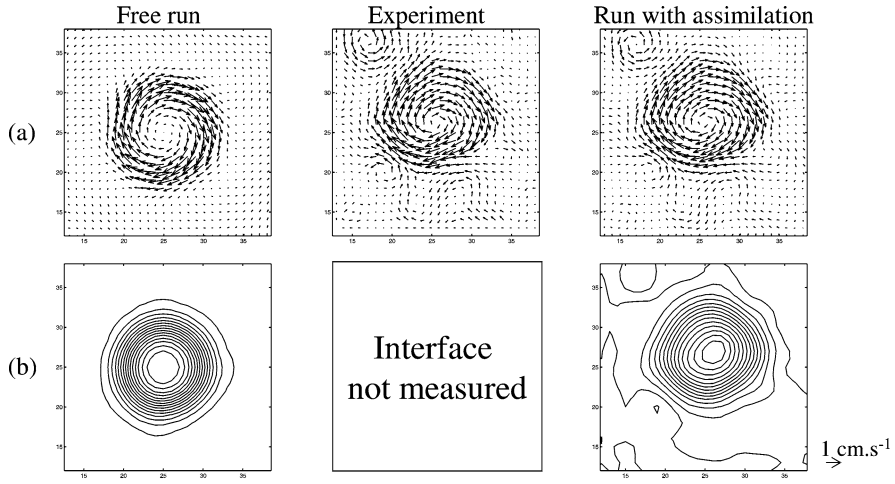

Fig. 1. Baroclinic instability of a two-layer vortex: velocity field in the top layer (a) and interface depth (b) at $t = 75$ s in the free run, in the experiment and in the simulation performed with data assimilation every 22 s. For clarity, only 25^2 vectors are plotted. The rms measurement error is about 0.5 mm·s^{-1}.

Fig. 1. Instabilité barocline d'un tourbillon bi-couche : champ de vitesse dans la couche supérieure (a) et profondeur de l'interface (b) au temps $t = 75$ s dans la simulation libre, l'expérience et la simulation avec assimilation de données toutes les 22 s. Pour plus de clarté, seulement 25^2 vecteurs sont représentés. L'erreur de mesure rms est de l'ordre de 0.5 mm·s^{-1}.

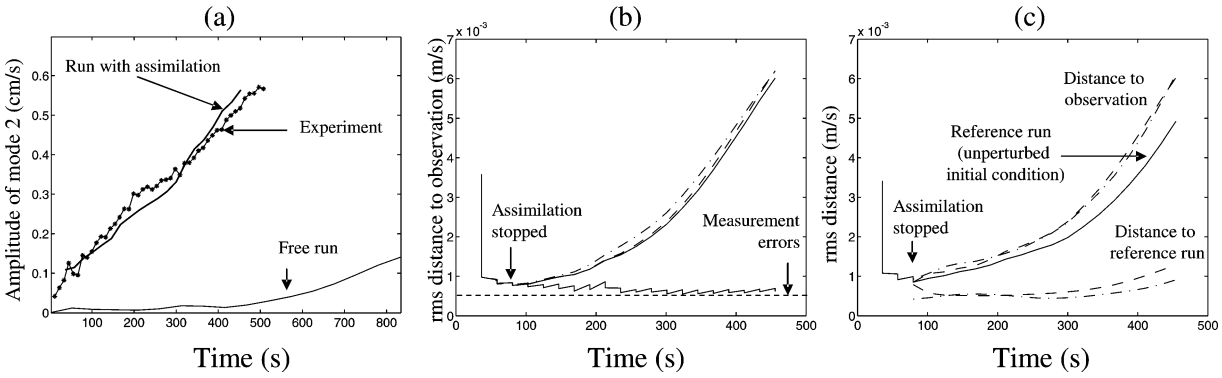

Fig. 2. (a) Amplitude of baroclinic mode 2 in the top layer as a function of time in the experiment, in the free simulation and in the simulation performed with data assimilation every 22 s. (b) Value of the rms distance between the simulated and measured velocity fields in the top layer as a function of time in the simulation performed with data assimilation every 22 s and in the simulation where data assimilation is stopped at $t = 75$ s. 200^2 grid points are used in both layers. The results obtained in two other test runs are also plotted: simulation with doubled viscosity coefficient (dashed line) and simulation with additional friction (dot-dashed line). The Ekman friction coefficient C_f is taken as equal to 1.4×10^{-3} s^{-1} in the bottom layer and 5.6×10^{-3} s^{-1} in the top layer. These values are those obtained assuming rigid upper and lower boundaries. (c) Value of the rms distance between the simulated and measured velocity fields in the top layer as a function of time when assimilation is stopped at $t = 75$ s. 100^2 grid points are used in both layers. Two test runs were performed using a perturbed initial condition at time $t = 75$ s. In the first test run (dashed line), the velocity field $\mathbf{u}$ in each layer is replaced at time $t = 75$ s by $\mathbf{u}_{\text{obs}} + \mathbf{R}(\mathbf{u} - \mathbf{u}_{\text{obs}})$, where $\mathbf{u}_{\text{obs}}$ is the observed velocity field and $\mathbf{R}$ is the 90° rotation operator. In the second test run (dot-dashed line), a large friction coefficient is imposed ($C_f = 1.4 \times 10^{-2}$ s^{-1} in the bottom layer and 5.6×10^{-2} s^{-1} in the top layer) from $t = 0$ to $t = 75$ s only, resulting in a slightly perturbed initial condition at time $t = 75$ s. The rms distance between the test runs and the reference run is also plotted.

Fig. 2. (a) Amplitude du mode 2 barocline dans la couche supérieure en fonction du temps dans l'expérience, dans la simulation libre et dans la simulation avec assimilation de données toutes les 22 s. (b) Valeur de la distance rms entre les champs de vitesse simulé et observé dans la couche supérieure en fonction du temps, dans la simulation avec assimilation de données toutes les 22 s et dans la simulation obtenue en cessant l'assimilation de données au temps $t = 75$ s. 200^2 points de grille sont utilisés dans chaque couche. Les résultats obtenus dans deux cas tests sont également tracés : simulation avec un coefficient de viscosité double (tirets) et simulation avec friction additionnelle (trait d'axe). Le coefficient de friction d'Ekman est pris égal à 1.4×10^{-3} s^{-1} dans la couche inférieure et 5.6×10^{-3} s^{-1} dans la couche supérieure. Ces valeurs sont celles obtenues en supposant la présence de parois rigides au fond et en surface. (c) Valeur de la distance rms entre les champs de vitesse simulé et mesuré dans la couche supérieure en fonction du temps lorsque l'assimilation est interrompue au temps $t = 75$ s. Dans un premier cas test (tirets), le champ de vitesse $\mathbf{u}$ dans chaque couche est remplacé au temps $t = 75$ s par $\mathbf{u}_{\text{obs}} + \mathbf{R} - (\mathbf{u} - \mathbf{u}_{\text{obs}})$, où $\mathbf{u}_{\text{obs}}$ est le champ de vitesse observé et $\mathbf{R}$ est l'opérateur de rotation à 90°. Dans un second cas test (trait d'axe), un coefficient de friction important est imposé ($C_f = 1.4 \times 10^{-2}$ s^{-1} dans la couche inférieure et 5.6×10^{-2} s^{-1} dans la couche supérieure) de $t = 0$ à $t = 75$ s seulement, fournissant une condition initiale légèrement perturbée au temps $t = 75$ s. La distance rms entre les cas tests et la simulation de référence est également tracée.

The rms distance between the forecast and measured velocity fields is plotted in Fig. 2(b). After a few assimilation cycles, this distance remains of the order of 0.6 mm·s^{-1}, close to the experimental errors (3% of the maximum velocity, i.e., about 0.5 mm·s^{-1}). Similar agreement is obtained in both layers.

The state vector obtained at a given time can be used as an initial condition to test the free model. To do so, we stop the assimilation at time $t = 75$ s and measure the growth of the rms distance between the laboratory experiments and the free model run with this new initial state, as shown in Fig. 2(b). This growth can be due either to the amplification of small initial errors, or to limitations of the dynamical model. The sensitivity to the initial condition is actually not the dominant effect, as observed in Fig. 2(c). It is clear in this figure that the divergence of the model from the experimental reality is not sensitive, over the short term, to small variations in the initial condition. For instance, the results are unchanged when the velocity field $\mathbf{u}$ in each layer is replaced at time $t = 75$ s by $\mathbf{u}_{\text{obs}} + \mathbf{R}(\mathbf{u} - \mathbf{u}_{\text{obs}})$, where $\mathbf{u}_{\text{obs}}$ is the observed velocity field and $\mathbf{R}$ is the 90° rotation operator. The model diverges from reality on a timescale of around 3000 s, which is about 30 times the typical advection timescale of the flow $2R/U \simeq 100$ s (where $U \simeq 1$ cm·s^{-1} is the order of magnitude of the velocity within the

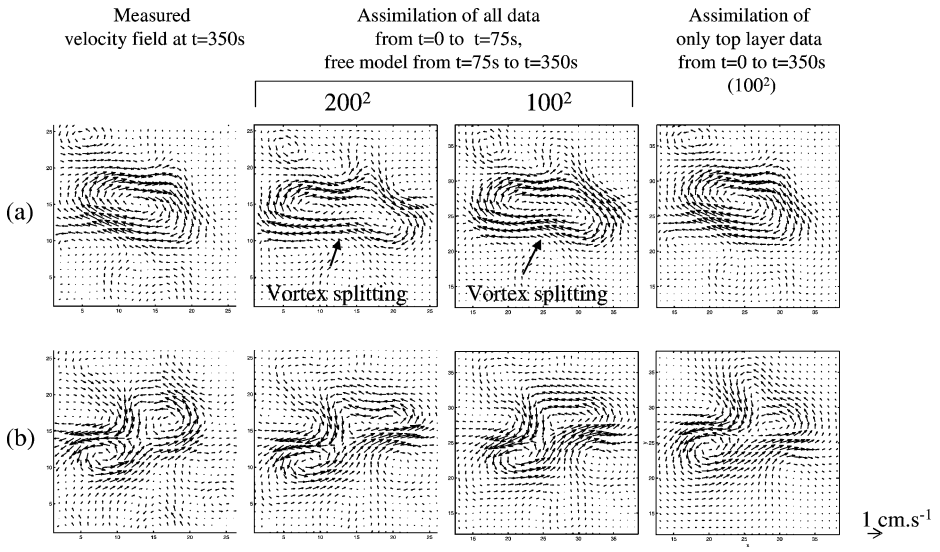

Fig. 3. Velocity field in the top (a) and bottom (b) layers at $t = 350$ s obtained in the experiment and in the simulation using different assimilation scenarios: assimilation of all data switched off at $t = 75$ s (note that the vortex splitting occurs faster than in the experiment, independently of the resolution); assimilation using only top layer data until $t = 350$ s (note that the bottom layer is well reconstructed). For clarity, only 25^2 vectors are plotted in all cases.

Fig. 3. Champ de vitesse dans la couche supérieure (a) et dans la couche inférieure (b) au temps $t = 350$ s obtenus expérimentalement et dans la simulation avec différents scénarios d'assimilation : assimilation de toutes les données jusqu'au temps $t = 75$ s (noter que la rupture du tourbillon intervient plus rapidement que dans l'expérience, indépendemment de la résolution) ; assimilation des données de surface jusqu'au temps $t = 350$ s (noter la reconstruction de la couche inférieure). Pour plus de clarté, seulement 25^2 vecteurs sont représentés dans chaque cas.

flow). The model error is therefore about $1/30$ of the dominant advective term. This error is actually small but seems to be systematic.

The results are similar when 100^2 or 200^2 numerical grid points are used in each layer. The effect of dissipation and friction was also investigated in various test runs. The rms distance to observations obtained in the most representative of these test runs is plotted in Fig. 2(a). The results show that the model errors persist when the numerical viscosity coefficient is changed or when an Ekman friction term is added in the momentum equation. We notice that, in all cases, vortex splitting occurs faster than in the experimental reality (Fig. 3). It is therefore likely that the basic simplifying assumptions of the hydrostatic, two-layer shallow-water formulation, rather than resolution, dissipation or friction problems, are responsible for the limitations of the model. For instance, the interface between the layers may have a finite thickness in reality, leading to effects that cannot be reproduced in the two-layer simulation. Also, the hydrostatic approximation may slightly enhance the growth of baroclinic instability, as shown in the theoretical study of non-hydrostatic effects by Stone [6].

In the last stage of our testing procedure, we perform assimilation using only upper layer data and check how the behavior of the lower layer is reconstructed. The results are shown in Fig. 3. Although some local discrepancies are observed in the bottom layer compared to the measured velocity field, the global flow field is well reproduced.

4. Conclusion

The results reported in the present letter illustrate the interest of data assimilation at the laboratory scale:

(i) Thanks to data assimilation, a complete description of the experimental flow fields is obtained, including the non-measured variables. Data assimilation can thus be used as a complementary tool for a better physical

analysis of experimental flows. In particular, potential vorticity anomalies can be calculated from the model output, providing quantities which are generally impossible to measure but which are crucial to a better understanding of the physics of layered flows.

(ii) The obtained flow field can be used as an initial condition to test the numerical model. In our test cases, the sensitivity of the model trajectory to weak variations in the initial condition is weak. Then even weak model errors can be detected, of the order of $1/30$ of the dominant inertial term in the present case. The most probable sources of error are the hydrostatic approximation or the two-layer formulation of the equations.

(iii) The accuracy of the assimilation scheme can also be analysed in detail. The present study shows, for instance, how the assimilation scheme is able to reconstruct the velocity field of the lower layer from observation of the upper layer.

Many other tests can of course be performed with the available data using various dynamical models and/or assimilation schemes. Possible improvement by non-hydrostatic models would be of particular interest. The study of other processes is in progress, involving the instability of boundary currents, gravity currents on a slope and current/topography interaction.

Acknowledgements

This study has been sponsored by EPSHOM, contract Nr. 9228. We acknowledge the kind support of Y. Morel for the implementation of the MICOM model, and of J.M. Brankart, P. Brasseur and C.E. Testut for the implementation of the SEEK assimilation scheme.

References

[1] N. Serra, S. Sadoux, I. Ambar, D. Renouard, Observation and laboratory modeling of meddy generation at Cape St Vincent, J. Phys. Oceans 32 (2002) 3–25.
[2] A. Fincham, G. Delerce, Advanced optimization of correlation imaging velocimetry algorithms, Experim. Fluids 29 (2000) S13–S22.
[3] R. Bleck, D. Boudra, Wind driven spin-up in eddy-resolving ocean models formulated in isopycnic coordinates, J. Geophys. Res. 91 (1986) 7611–7621.
[4] D. Pham, J. Verron, M. Roubaud, A singular evolutive extended Kalman filter for data assimilation in oceanography, J. Marine Sci. 16 (3–4) (1998) 323–340.
[5] P. Brasseur, J. Ballabrera-Poy, J. Verron, Assimilation of altimetric data in the mid-latitude oceans using the singular evolutive extended Kalman filter with an eddy-resolving, primitive equation model, J. Marine Sci. 22 (1999) 269–294.
[6] P.H. Stone, Baroclinic instability under non-hydrostatic conditions, Part 4, J. Fluid Mech. 45 (1971) 659–671.